Cell, Vol. 108, 345–356, February 8, 2002, Copyright ©2002 by Cell Press

Structural Basis for E2-Mediated SUMO Conjugation Revealed by a Complex between Ubiquitin-Conjugating Enzyme Ubc9 and RanGAP1

Victor Bernier-Villamor,[1] Deborah A. Sampson,[2] Michael J. Matunis,[2] and Christopher D. Lima[1,3]
[1]Biochemistry Department
Structural Biology Program
Weill Medical College of Cornell University
New York, New York 10021
[2]Department of Biochemistry and Molecular Biology
Bloomberg School of Public Health
Johns Hopkins University
Baltimore, Maryland 21205

Summary

E2 enzymes catalyze attachment of ubiquitin and ubiquitin-like proteins to lysine residues directly or through E3-mediated reactions. The small ubiquitin-like modifier SUMO regulates nuclear transport, stress response, and signal transduction in eukaryotes and is essential for cell-cycle progression in yeast. In contrast to most ubiquitin conjugation, the SUMO E2 enzyme Ubc9 is sufficient for substrate recognition and lysine modification of known SUMO targets. Crystallographic analysis of a complex between mammalian Ubc9 and a C-terminal domain of RanGAP1 at 2.5 Å reveals structural determinants for recognition of consensus SUMO modification sequences found within SUMO-conjugated proteins. Structure-based mutagenesis and biochemical analysis of Ubc9 and RanGAP1 reveal distinct motifs required for substrate binding and SUMO modification of p53, IκBα, and RanGAP1.

Introduction

Ubiquitin (Ub) and ubiquitin-like (Ubl) modifiers are ~100 amino acid proteins that modulate protein function through posttranslational covalent attachment to lysine residues within targeted proteins. The Ub/Ubl-conjugated state of proteins has been linked to critical cellular pathways including differentiation, apoptosis, the cell cycle, and responses to stress (Muller et al., 2001; Melchior, 2000; Hershko and Ciechanover, 1998; Hochstrasser, 1996; Laney and Hochstrasser, 1999; Saitoh et al., 1997). SUMO-1 (small ubiquitin-related modifier; also known as PIC1, UBL1, Sentrin, GMP1, and Smt3) is a member of the ubiquitin and ubiquitin-like superfamily. Although SUMO-1 shares some sequence and structural similarity to ubiquitin, the cellular functions for each family are unique. Ubiquitinated proteins are generally polyubiquitinated and targeted to the 26S proteosome for degradation (Hershko and Ciechanover, 1998). Sumoylated substrates are not generally polysumoylated, nor are they targeted for degradation. SUMO modification alters target protein function through changes in activity, cellular localization, or protection from ubiquitination.

[3]Correspondence: lima@pinky.med.cornell.edu

Saccharomyces cerevisiae Smt3 was the first SUMO ortholog to be identified (Meluh and Koshland, 1995). Smt3 modification appears critical for septin ring formation, chromosomal segregation, and progression of the cell cycle through G_2-M (Johnson and Blobel, 1999; Takahashi et al., 1999; Tanaka et al., 1999; Li and Hochstrasser, 1999). Mammals contain three known SUMO proteins that include classical SUMO-1 and two others, SUMO-2 and SUMO-3, that share roughly 50% sequence identity with SUMO-1. We will use SUMO to describe the system and refer by name to protein components.

Several SUMO-conjugated proteins have been identified that modulate critical cellular pathways. Sumoylation of mammalian RanGAP1 occurs on Lys526, a modification required for nucleocytoplasmic transport and for its association with Nup358 (RanBP2) at the nuclear pore complex (Matunis et al., 1996; Mahajan et al., 1997). IκBα sumoylation occurs on Lys21, the same residue targeted for ubiquitination, thus protecting IκBα from degradation, a process that leads to NFκB nuclear translocation (Desterro et al., 1998). Sumoylation of p53 Lys386 does not directly protect it from ubiquitination, but enhances p53 transcriptional activity through a mechanism that remains unclear (Rodriguez et al., 1999; Gostissa et al., 1999). PML, PML-RAR, and SP100 nuclear localization (Kamitani et al., 1998; Sternsdorf et al., 1997), centromere segregation (Tanaka et al., 1999), and septin ring formation (Johnson and Blobel, 1999; Takahashi et al., 1999) are among several other pathways modulated by SUMO conjugation, indicative of a large and varied role for this process in the cell (Melchior, 2000).

The mechanisms utilized to attach ubiquitin and ubiquitin-like modifiers to cellular proteins share many similarities and some important differences. All Ub/Ubl conjugation results in isopeptide bond formation between a protein lysine ϵ amino group and the Ub/Ubl modifier C terminus (Hershko and Ciechanover, 1998). Full-length Ub/Ubl is first proteolytically processed at its C terminus, producing the conserved Ub/Ubl C-terminal diglycine (Gly-Gly) motif. The Ub/Ubl C terminus is then adenylated by E1 enzymes and transferred to a conserved E1 cysteine to form an E1-Ub/Ubl thioester adduct. The Ub/Ubl-E1 thioester is subsequently transferred to a conserved cysteine within E2. E2 then utilizes the energy stored in the thioester bond to enable Ub/Ubl transfer to E3 molecules or to directly conjugate the Ub/Ubl modifier to a lysine ϵ amino group within a protein target.

Ubiquitin conjugation utilizes unique combinations of numerous E2 and E3 factors to direct catalysis and ensure specificity during conjugation (Hershko and Ciechanover, 1998). In contrast, Ubc9 is the only known SUMO E2 enzyme (Seufert et al., 1995; Johnson and Blobel, 1997), and Ubc9 is apparently sufficient for SUMO conjugation since all identified substrates can be specifically modified in vitro using only E1, Ubc9, mature SUMO, and ATP. Interestingly, recent reports identified two yeast E3-like ring finger proteins, Siz1

and Siz2, that enhance E2-mediated sumoylation of the septins (Johnson and Gupta, 2001; Takahashi et al., 2001), and another report identified an E3-like ring finger protein PIAS that enhanced p53 sumoylation (Kahyo et al., 2001). Siz1, Siz2, and PIAS proteins are related by sequence and have been assigned the SP-ring acronym, for Siz-PIAS-ring finger motifs (Hochstrasser, 2001). The identified SP-ring factors do not alter Ubc9 specificity, suggesting that these E3s regulate SUMO conjugation by increasing affinity between Ubc9 and substrate.

Most SUMO-modified proteins contain the tetrapeptide motif Ψ-K-x-D/E where Ψ is a hydrophobic residue, K is the lysine conjugated to SUMO, x is any amino acid, and D or E is an acidic residue. The observed consensus motif within SUMO conjugation targets is unique since similar consensus sequences have not been uncovered in ubiquitin conjugation pathways. Substrate specificity appears to be derived directly from Ubc9 and the respective substrate motif since no other cofactors are needed in vitro to observe Ubc9 catalytic specificity.

Structural data has not been available for any ubiquitin or SUMO conjugating enzyme-substrate complex, highlighting a significant gap in our understanding for ubiquitin and ubiquitin-like modifier transfer from E2 or E3 enzymes to a substrate lysine. To determine the molecular basis for E2-dependent transfer mechanisms and to elaborate interactions utilized by Ubc9 for substrate recognition and catalytic activity, we have structurally characterized a complex between Ubc9, the SUMO conjugating enzyme, and RanGAP1. Structure-based mutagenesis of the Ubc9-RanGAP1 interface combined with assays for p53, IκBα, and RanGAP1 SUMO conjugation have enabled Ubc9-substrate interactions to be generalized, highlighting a critical and central role for the SUMO motif in Ubc9-mediated conjugation.

Results and Discussion

Structure Determination of the Ubc9-RanGAP1 Complex

Human Ubc9 and a C-terminal fragment of mouse RanGAP1(420–589)p were purified to isolate a complex previously characterized as a minimal functional domain for E2-SUMO conjugation (Sampson et al., 2001). Selenomethionine-substituted protein was isolated, crystallized, and used in a 3 wavelength MAD experiment to obtain phases (Hendrickson, 1991). A single complex crystallized per asymmetric unit (ASU) (83% solvent content). This facilitated density modification and produced interpretable electron density (Table 1; see Experimental Procedures).

A model for Ubc9 and RanGAP1 was built and refined to 2.8 Å to an R factor and R_{free} of 0.30 and 0.36, respectively. A second crystal form was identified in the interim that diffracted anisotropic X-rays to 2.3 Å. The model was used in molecular replacement calculations with the second data set (two complexes per ASU) and refined to 2.5 Å. The second crystal form contained an intercomplex disulfide bridge between Ubc9 Cys138 and RanGAP1 Cys575 (from complex 1 to 2 and 2 to 1). These bonds did not affect changes in Ubc9 or the interface between Ubc9 and RanGAP1, although it did result in structural perturbations for RanGAP1 residues 573–576, residues observed in helical conformation in the first crystal form. The structure has been refined to an R factor and R_{free} of 0.223 and 0.301, respectively. A section of simulated annealing omit map electron density is presented in Figure 1 (Brunger et al., 1998; Table 1; see Experimental Procedures).

Structures of Ubc9 E2 and RanGAP1

A structure for human Ubc9 has been described (Tong et al., 1997). We also crystallized and determined the structure for human Ubc9 at 2.0 Å by molecular replacement. This model was used to dock Ubc9 into the experimental RanGAP1-Ubc9 electron density prior to refinement and manual rebuilding. Ubc9 and other ubiquitin E2 family members encode a similar fold and active site cysteine. Briefly, most E2 enzymes contain an N-terminal α helix followed by a five- to seven-stranded β sheet, the loop containing the catalytic cysteine, followed by three C-terminal α helices (Figures 2A and 2B). Ubc9 does not undergo significant conformational changes in complex with RanGAP1 (0.69 $Å^2$ root mean square deviation [rmsd] over amino acids 3–158 to uncomplexed Ubc9). The largest differences observed occur in helix C, a region in direct contact with RanGAP1.

The C-terminal domain of mammalian RanGAP1 has not been previously reported, although the structure for the *S. pombe* RanGAP1 N-terminal domain has been solved (Hillig et al., 1999). Vertebrate and fungal RanGAP1 proteins share roughly 35% sequence identity in their N-terminal domain, but differ because yeast RanGAP1 orthologs do not contain the C-terminal domain that is sumoylated and required for RanGAP1 localization at the vertebrate nuclear pore complex.

The RanGAP1(420–589)p structure reveals a domain composed almost entirely of helical substructures with one noted exception, the peptide containing the lysine required for SUMO conjugation. The SUMO consensus motif is observed in extended conformation between helices F and G (Figure 2C). A structural homology search calculated with DALI (Holm and Sander, 1993) revealed similarities to ~100 amino acid helical-repeat domains sharing 6%–12% sequence identity to RanGAP1 from proteins such as clathrin assembly lymphoid myeloid leukemia protein, the h-ras fragment (p21) of son of sevenless-1, protein phosphatase pp2a, karyopherin β-1, and pumilio, among many others. None share sequence or structural homology with the RanGAP1 SUMO motif, indicating architectural rather than functional significance to these similarities. PFAM and PSI-Blast, programs that rely heavily on sequence search algorithms, did not uncover these relationships.

Structure of the RanGAP1-Ubc9 Complex

Elucidation of the Ubc9-RanGAP1 complex revealed several critical interactions between Ubc9 and RanGAP1 that included the molecular basis for Ubc9 recognition of the RanGAP1 Ψ-K-x-D/E consensus motif. Although continuous, the interface between RanGAP1 and Ubc9 can be most simply described in two parts. The first includes interactions between RanGAP1 helices H and F and Ubc9 surfaces emanating mainly from helix C. The second part includes interactions between the consensus RanGAP1 sumoylation motif (-LKSE-) and Ubc9

Table 1. Crystallographic Data

Resolution (Å)	Wavelength (Å)	Reflections (Unique/Total)	Coverage (%)	(I/σ)	R_{sym}[a]
25–2.8	0.9793 (edge)	50,956/678,527	84.8 (67.7)	10.4 (2.5)	0.102 (0.43)
25–2.8	0.9788 (peak)	48,413/551,627	80.5 (60.0)	10.4 (2.8)	0.085 (0.42)
25–2.8	0.9712 (remote)	48,072/554,374	80.1 (60.5)	9.7 (2.7)	0.090 (0.44)
25–2.5	0.9790 (native)	27,902/274,090	96.2 (92.2)	12.0 (3.1)	0.080 (0.34)

Anomalous Diffraction Ratios[b] (25–2.8 Å)

	Edge	Peak	Remote
Edge	0.102 (0.241)	0.052 (0.175)	0.063 (0.189)
Peak		0.111 (0.237)	0.057 (0.169)
Remote			0.107 (0.248)

FOM[c] (25–2.8 Å)

SOLVE (Acentric/Centric)	0.28 (0.10)/0.24 (0.10)
RESOLVE (Acentric/Centric)	0.53 (0.24)/0.58 (0.17)

Refinement (25–2.5 Å)

Number of reflections $> 0.0\sigma$	27,248	Rms deviations[d]	
Nonhydrogen atoms		Bond length (Å)	0.007
Protein	4,932	Bond angles (°)	1.30
Sulfate	20	B main/side chain (Å^2)	1.71/2.21
Water	585		
R_{cryst}[e]	0.223		
R_{free}[f]	0.300		

MAD data completeness treats Bijvoët mates independently. Numbers in parentheses indicate outer shell statistics.
[a] $R_{sym} = \Sigma|I - \langle I\rangle|/\Sigma I$, where I is the observed intensity, $\langle I\rangle$ is the average intensity.
[b] Anomalous diffraction ratios $= \langle\Delta|F|^2\rangle^{1/2}$, where $\Delta|F|$ is the absolute value of the Bijvoët (diagonal elements) or dispersive difference (off diagonal elements).
[c] Figure of merit $= |F(hkl)_{best}|/F(hkl)$
[d] Root mean square deviations from ideal geometry and B factors for bonded atoms.
[e] R_{cryst} R based on 95% of the data.
[f] R_{free} R based on 5% of the data withheld for crossvalidation.

surfaces that include the catalytic cysteine, strands 6 and 7, and the loop preceding helix C (Figures 2, 3, and 4).

The complex buries roughly 1500 Å^2 of total accessible surface area (1.4 Å probe radius), accounting for ~9% of the total area calculated for the two molecules alone (Nicholls et al., 1991). The RanGAP1 SUMO consensus motif is extruded from the helical domain, enabling simple calculation of accessible surface area buried by the SUMO motif. Leu525 to Glu528 was deleted from RanGAP1, and 460 Å^2 of buried accessible surface area was lost. The calculation was repeated for Ubc9 and the tetrapeptide motif, resulting in 550 Å^2 of buried accessible surface area, roughly one-third of the total. A detailed description of these interactions follows.

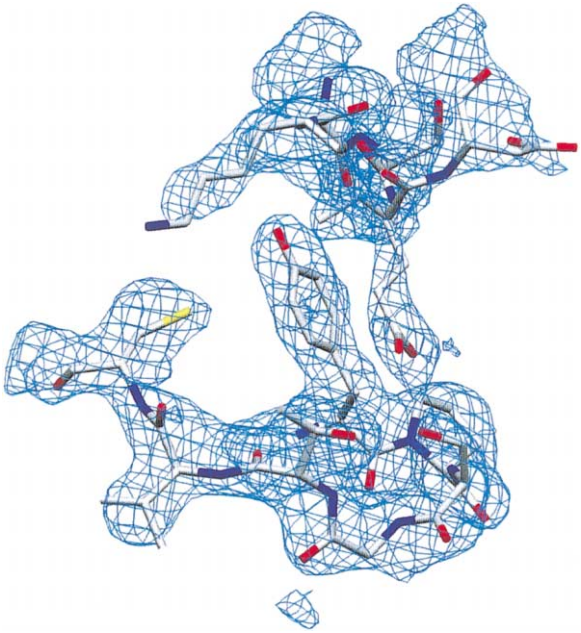

Figure 1. Electron Density Map for the RanGAP1-Ubc9 Complex

Simulated annealing omit map (1.0σ) centered on RanGAP1 Lys526 (top left) and Ubc9 Cys93 (bottom left). Figures generated with SETOR unless noted (Evans, 1993).

Ubc9 Recognition of the SUMO Consensus Motif

Almost all sumoylated proteins contain the tetrapeptide motif Ψ-K-x-D/E, where Ψ is a hydrophobic residue, K is the lysine to which SUMO is conjugated, x is any amino acid, and D or E is an acidic residue. The RanGAP1 consensus peptide (525–528) is observed in extended β-like conformation, although hydrogen bonding patterns to the peptide main chain do not support this configuration directly. The motif begins with the hydrophobic residue Ψ (Leu525 in RanGAP1). Leu525 side chain atoms are observed in VDW contact with atoms from Ubc9 residues Pro128, Ala129, Gln130, and Ala131. These interactions are not extensive since this Ubc9 surface is flat, indicating that hydrophobic residues at the Ψ position do not fit lock-and-key into a conserved pocket (Figure 4). Rather, sequence conservation at position 1 likely arises from exclusion of hydrophilic residues, an observation supported by the diversity of hydrophobic side chains located at this position (Melchior, 2000).

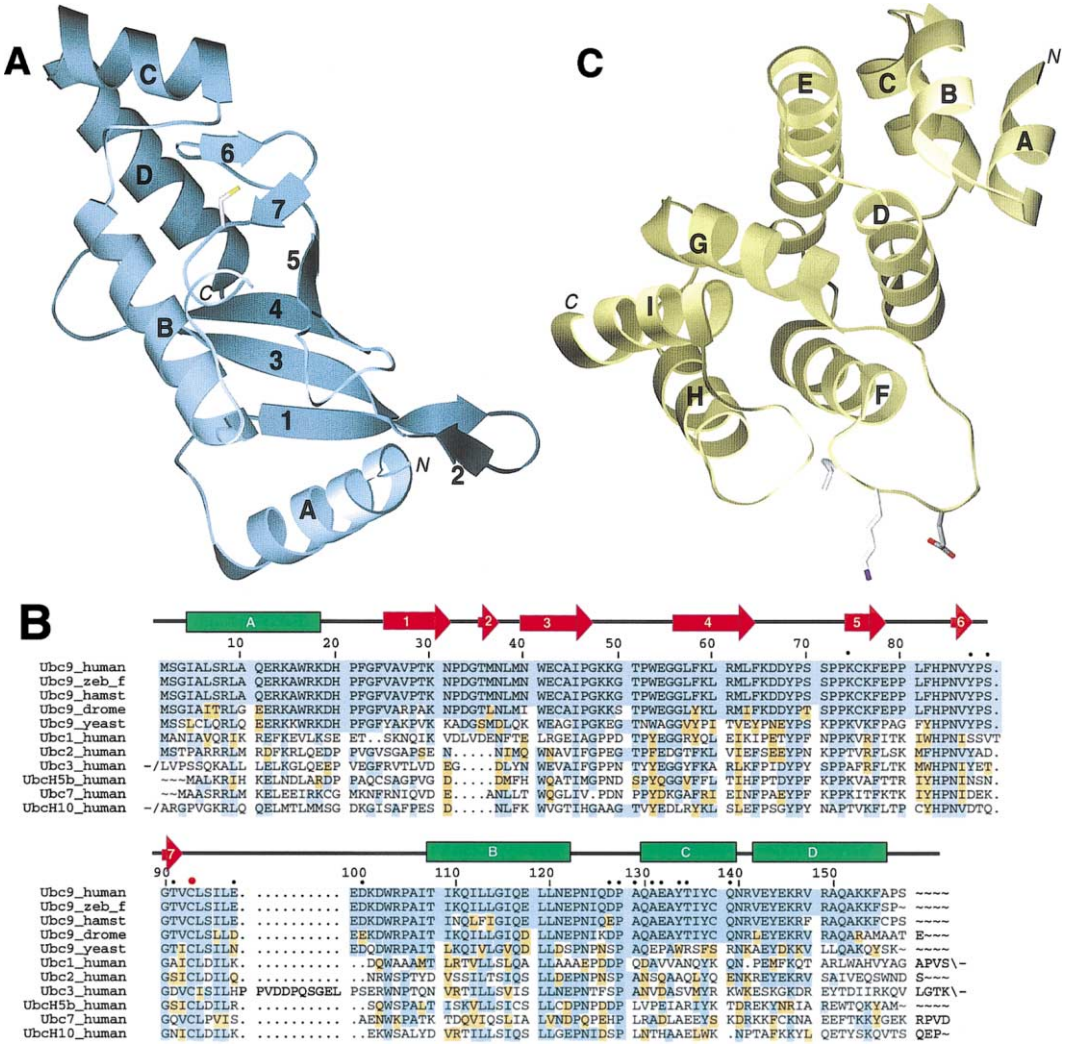

Figure 2. Ubc9 and RanGAP1 Ribbon Diagrams and Ubc9-E2 Sequence Alignment

(A) Ubc9 ribbon diagram and secondary structure assignment. Helices are lettered, strands are numbered. Cys93 is in solid bonds. N and C termini are denoted in italics.

(B) Structure-based sequence alignment for human Ubc9, zebra fish Ubc9, hamster Ubc9, *Drosophila* Ubc9, and *S. cerevisiae* Ubc9 and sequences for human Ubc1, Ubc2, Ubc3, UbcH5b, Ubc7, and UbcH10. Sequence identity is in blue shading, similarity is in yellow shading. Red and black dots over sequence indicate Cys93 and mutants, respectively. Numbering is for human Ubc9. Ubc9 secondary structure is indicated by arrows (strands numbered) and bars (helices lettered), as in (A).

(C) Ribbon diagram and secondary structure assignment for the C-terminal domain of RanGAP1. SUMO motif residues Leu525, Lys526, and Glu528 are in solid bonds.

The second residue of the motif is lysine, the strictly conserved amino acid that serves as the acceptor for SUMO and as the nucleophile during attack at the Ubc9-SUMO thioester. Lys526 is observed in a shallow groove created by backbone atoms from Ubc9 residues Asp127, Pro128, and Ala129 and side chain atoms from Ubc9 Asp127 and Tyr87 (Figures 4 and 5). The groove is mainly hydrophobic, comprised largely by interactions between aliphatic Lys526 side chain atoms and the Tyr87 aromatic ring. Asp127 and RanGAP1 Lys526 are within 2.7 Å hydrogen bonding distance, suggesting a catalytic role for Asp127 in Lys526 coordination during attack at the SUMO-Ubc9 thioester. The Lys526 Nϵ atom is also 2.6 Å away from an ordered water molecule and 3.5 Å away from the Sγ atom of the Ubc9 Cys93.

Side chains at the third consensus motif position are not conserved. The extended conformation of the peptide directs this amino acid side chain away from the surface of Ubc9. Although sequence conservation at the third position is low, a space between the lysine at position 2 and the acidic residue at position 4 would be required, serving to saddle the consensus peptide over Tyr87 through VDW interactions between Ser527 main chain atoms and side chain atoms from Tyr87.

The fourth position in the motif is almost always an acidic glutamate side chain, although some identified sites contain Asp or Asn, and more rarely, Pro. RanGAP1 Glu528 is observed within hydrogen bonding distance of Ser89 (2.5 Å), Thr91 (3.0 Å), and more distantly with Lys74 (3.6 Å) (Figure 4). Hydrophobic VDW interactions

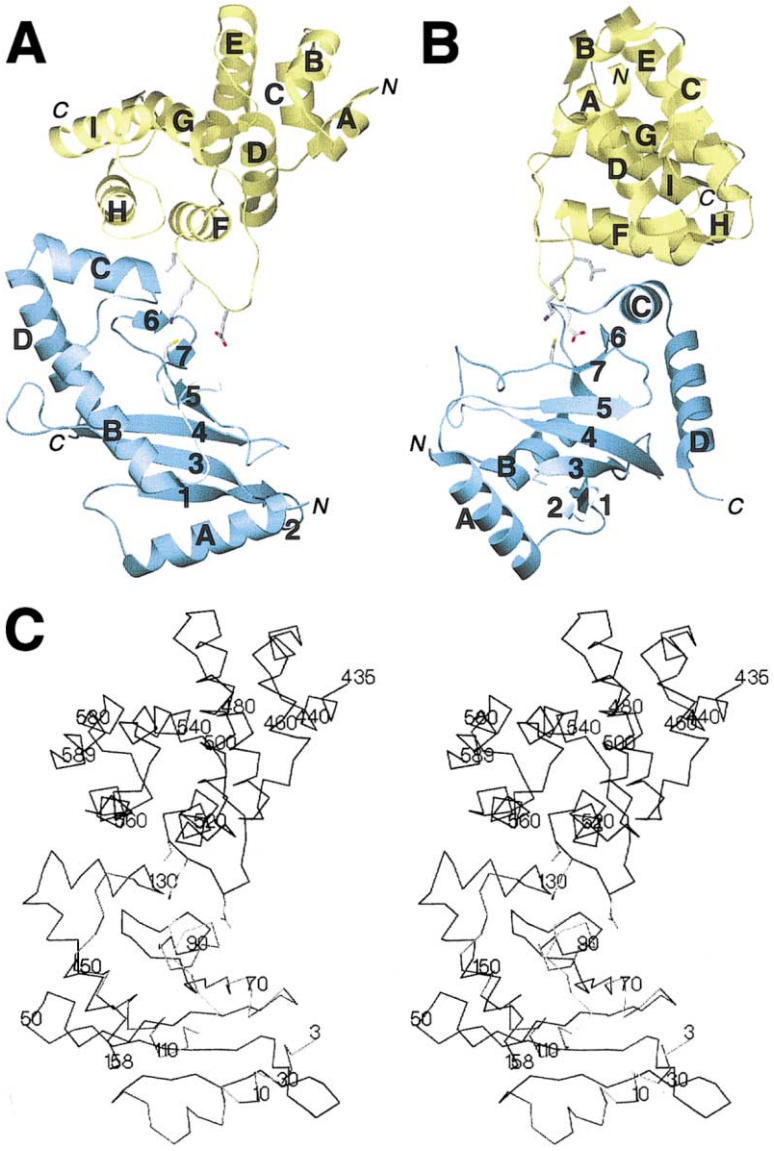

Figure 3. Ribbon and Stereo Diagrams for Ubc9-RanGAP1.

(A and B) Orthogonal ribbon representations with helices lettered and strands numbered, as in Figure 2. Ubc9 Cys93 and RanGAP1 Leu525, Lys526, and Glu528 are in solid bonds. N and C termini are denoted in italics. (C) Stereo image of the complex, as in (A).

are observed between Tyr87 and the aliphatic chain of Glu528, interactions that could partially explain the preference for the longer glutamic acid side chain at this position. Amino acids immediately preceding and following the motif are not in contact with Ubc9, suggesting that the Ψ-K-x-D/E motif is sufficient for Ubc9 modification. Structure and sequence-based mutagenesis used to test these observations will be discussed below.

Implications for SUMO and Ubiquitin Transfer

The active site observed in Ubc9 shares many similarities with those observed in other E2-conjugating enzymes and could thus serve as a model for other E2-substrate interactions. A commonly invoked mechanism for Ub/Ubl conjugation involves a general base that activates the nucleophilic acceptor lysine for ubiquitin and SUMO transfer. Residues surrounding the Ubc9 catalytic cysteine and RanGAP1 acceptor lysine, while coordinating the orientation of these residues, do not provide a general base or an environment that could specifically abstract a proton from the acceptor lysine. The Ubc9-SUMO thioester is extremely labile under physiological conditions, suggesting a suitably unstable bond that could facilitate direct transfer to the weakly nucleophilic lysine, if properly positioned, without involvement of other catalytic residues, thus resulting in the relatively stable isopeptide bond between the modifier and acceptor lysine.

RanGAP1 Lys526, the nucleophile and acceptor for SUMO, is within hydrogen bonding distance of Cys93, the catalytic Ubc9 cysteine, indicating that Lys526 is in an appropriate configuration to attack the E2-Ub/Ubl thioester during conjugation. Several residues near Cys93, such as Asp127, Asn85, and Tyr87, contain functional groups consistent with catalytic function. Several of these residues have been mutated (see below), and none completely block activity, indicating nonessential catalytic roles for most of these side chains. Conserved side chains in E2 alignments mostly occur in the hy-

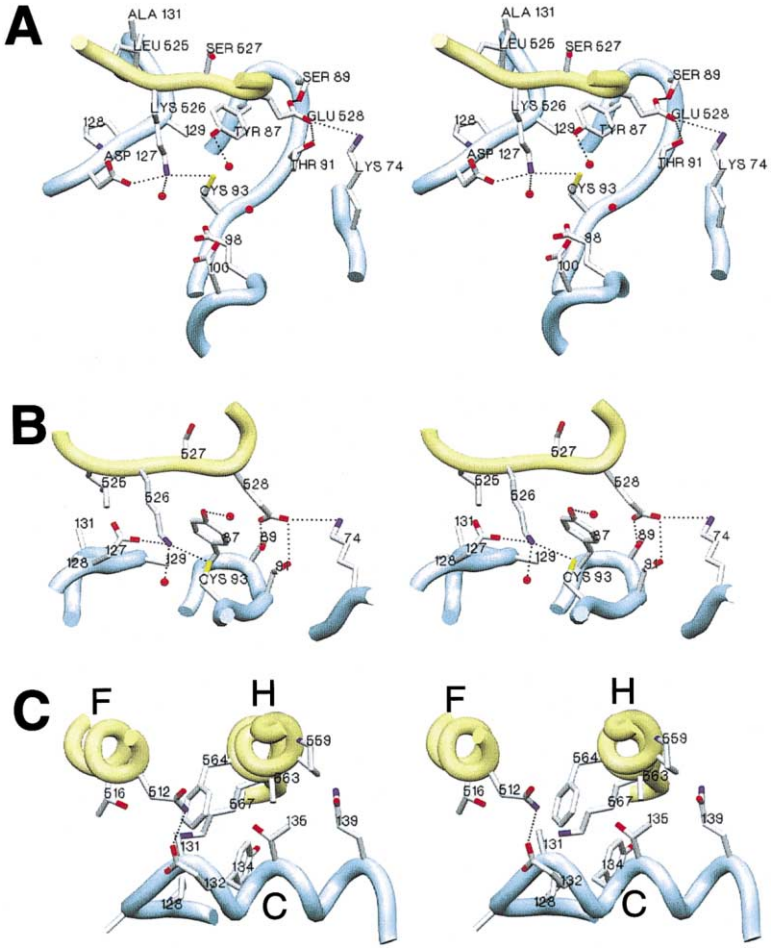

Figure 4. Stereo Images of Ubc9-RanGAP1 Interaction

(A and B) Orthogonal orientations of the RanGAP1 consensus motif in complex with Ubc9. Amino acids are indicated by type, number, or both. Ubc9 Glu98 and Asp100 are removed in (B).

(C) RanGAP1-Ubc9 interaction outside the motif recognition interface. Helices lettered for RanGAP1 (F and H) and Ubc9 (C). Backbone positions are represented by ribbon spline (RanGAP1 in yellow, Ubc9 in blue), theoretical hydrogen bonds are dotted lines, and waters are red spheres.

drophobic core and in loops that likely stabilize the fold (Figure 2B). Other conserved motifs suggestive of catalytic function include the HPN sequence motif observed at positions 83–85 and the less strictly conserved EPN motif at positions 122–124. Although untested, these regions appear to play primarily structural rather than catalytic roles. The HPN motif is involved in extensive side chain to main chain hydrogen bonding networks that form a scaffold within a channel implicated in coordination of the SUMO or ubiquitin diglycine motif (see below), and residues 122–124 are not located near the catalytic cysteine, but are near helices B and C, another area potentially involved in ubiquitin or SUMO interaction.

The Ubc9-RanGAP1 complex reveals a platform and unique position for the acceptor lysine within the Ubc9 catalytic site, suggesting a position for the SUMO C terminus and thioester adduct between Cys93 and Asp127, near the water molecule coordinated by Lys526 in Figure 4B. A channel is formed between the receptor peptide and Ubc9, one large enough to accommodate the Gly-Gly motif found at the end of all ubiquitin and ubiquitin-like modifiers (Figures 5A and 5B). A similar channel has been observed in the crystal structure of Smt3, the yeast SUMO ortholog, in complex with the yeast desumoylating enzyme Ulp1 (Mossessova and Lima, 2000). Smt3 coordinates (47% identical to human SUMO-1) were manually docked into the Ubc9-RanGAP1 complex (data not shown), suggesting that amino acid residues between Ubc9 helix B and C, as well as residues in the loop preceding Cys93, may play a role in coordinating an extended C-terminal diglycine motif.

The SUMO-Ubc9 complex proposed in our model is supported by recent NMR experiments that resolved a thioester complex between Ubc1 and ubiquitin (Hamilton et al., 2001). These studies indicate the channel may be utilized to coordinate the Gly-Gly motif and that helix B is a central element in E2-ubiquitin interaction. Comparing Ubc9-RanGAP1 to other E2-E3 or E2-E2 complexes (E6AP-UbcH7, c-Cbl-UbcH7, and Mms2/Ubc13) also supports this orientation for SUMO or ubiquitin in the complex (Huang et al., 1999; Zheng et al., 2000; VanDemark et al., 2001). These models, when taken together, utilize extensive E2 surfaces in their interactions while leaving open a large surface that could be available for ubiquitin or SUMO interaction (Figure 5E). Interestingly, E2 surfaces occluded in complexes with RanGAP1, Mms2, and collective E3s (E6AP and Cbl) are unique and nearly nonoverlapping, suggesting that several of these complexes could occur simultaneously, consistent with a role for E3-mediated E2-substrate interaction (Figures 5C–5E).

Functional Characterization of RanGAP1

SUMO conjugation assays have been utilized to probe structure-function relationships between RanGAP1 and

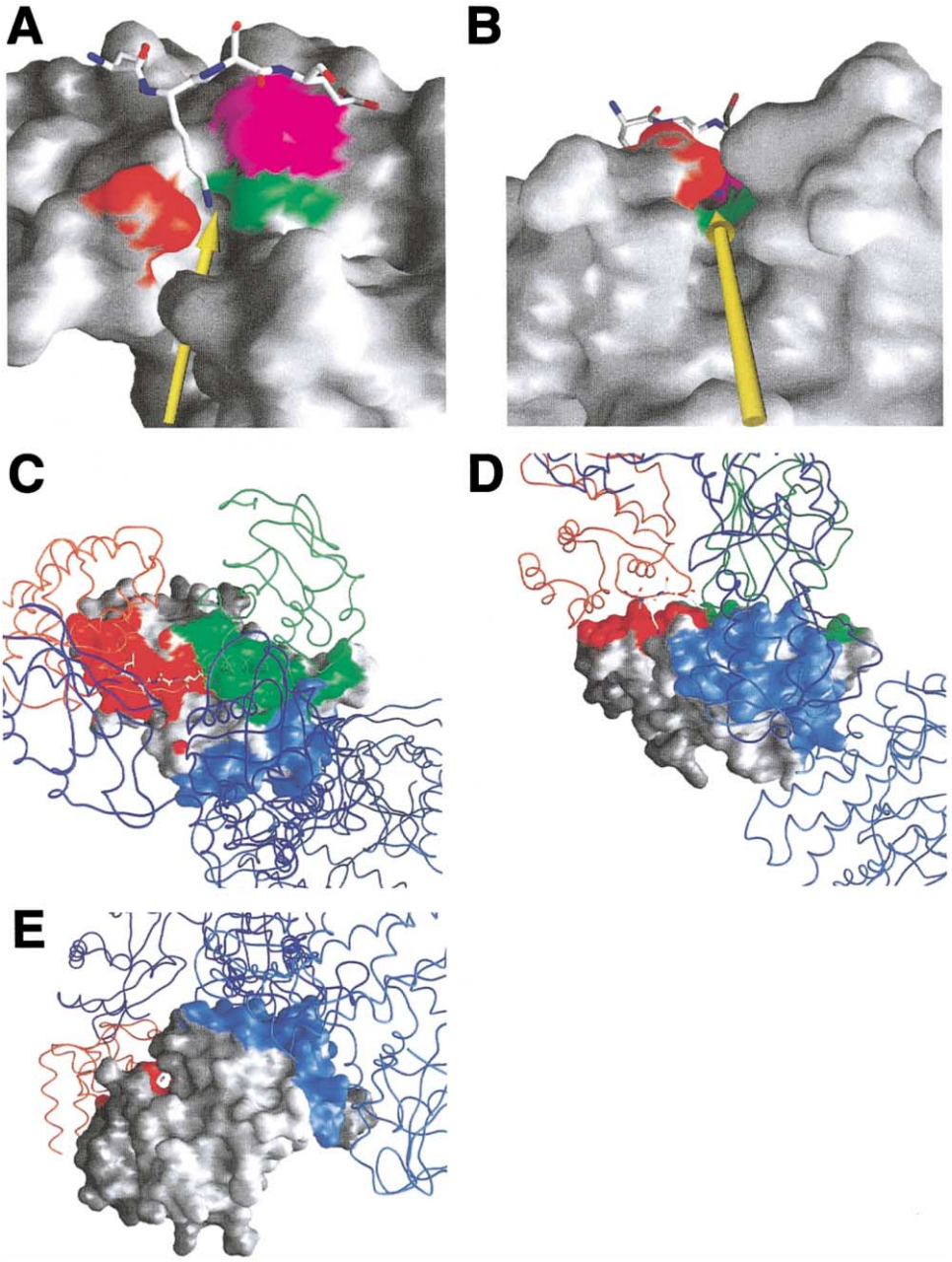

Figure 5. Models for Ubc9 Surfaces Utilized in Substrate, SUMO, E2, and E3 Binding

(A) Surface and bond representations for Ubc9 and the RanGAP1 SUMO tetrapeptide motif, respectively. Ubc9 Asp127 (red), Cys93 (green), and Tyr87 (pink) are indicated on the Ubc9 surface. The location of the channel discussed in the text is indicated by a yellow arrow.

(B) Orthogonal view of (A). RanGAP1 Lys526 Nϵ atom is visible beyond the yellow arrow.

(C–E) Orthogonal Ubc9 surface representations in complex with RanGAP1, Mms2, E6AP, and Cbl. The RanGAP1 SUMO motif is represented by solid bonds, RanGAP1(420–589)p as a red worm, the Cbl ring finger as a light blue worm, the E6AP Hect domain as a dark blue worm, and Mms2 as a green worm. Surface area buried in respective complexes is shown as a red surface (RanGAP1), a green surface (Mms2), and a blue surface (E6AP and Cbl, combined). E2s from each complex were aligned to Ubc9 by least-squares minimization on Cα atoms. Figures 5 and 7 were prepared with GRASP (Nicholls et al., 1991).

endogenous SUMO-conjugating enzymes (Sampson et al., 2001). Results from that study combined with further structure-based mutagenesis from this study reveal mutations in the sumoylation motif and in helix H that dramatically disrupt sumoylation. RanGAP1 mutations with no observable defects in conjugation included residues in helix F, residues stabilizing the conformation of the SUMO motif, and several residues in helix H (Figures 6A, 7C, and 7D).

L524A disrupts sumoylation, and although Leu524 does not interact with Ubc9 directly, it likely anchors the RanGAP1 consensus motif (525–528) within its hydrophobic core, thus stabilizing the conformation of the SUMO motif. L525A probably disrupts hydrophobic

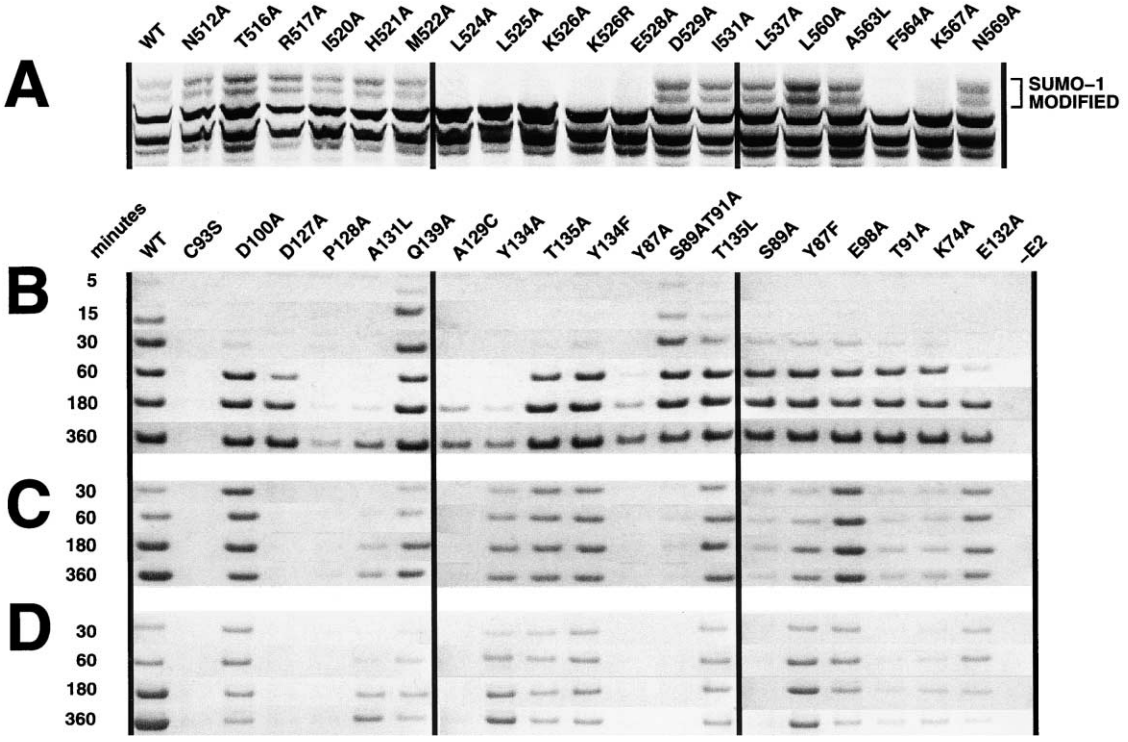

Figure 6. SDS-PAGE Analysis for SUMO Conjugation and Product Formation Utilizing Wild-Type and Mutant RanGAP1 and Ubc9

(A) RanGAP1 SUMO conjugation assay by endogenous conjugating enzymes with mutant and wild-type RanGAP1.

(B) RanGAP1(420–589)p SUMO conjugation using wild-type and mutant Ubc9.

(C) p53(320–393)p SUMO conjugation using wild-type and mutant Ubc9.

(D) IκBα SUMO conjugation using wild-type and mutant Ubc9. Wild-type and mutant enzymes are denoted by WT or mutation (i.e., C93S for cysteine to serine at residue 93). Panels in (B)–(D) were constructed with cut-outs from several Coomassie-stained SDS-PAGE gels containing respective sumoylation products (see Experimental Procedures).

VDW interactions between Ubc9 and RanGAP1, although alanine has been observed at this position in at least two confirmed SUMO targets (Melchior, 2000). K526A and K526R both disrupt sumoylation by removal of the acceptor lysine, although K526R still exhibited wild-type binding affinities for Ubc9. E528A mutation also disrupts SUMO transfer, and as explained previously, the glutamic acid makes VDW contacts with Tyr87 and is within hydrogen bonding distance to Ubc9 Lys74, Ser89, and Thr91. These mutations reveal an essential role for the consensus motif during Ubc9-mediated conjugation.

F564A and K567A reveal critical interactions between RanGAP1 and Ubc9 that are distant from direct interactions with the consensus SUMO motif and indicate RanGAP1 adaptations to increase Ubc9 interaction (Figure 4C). F564A is predicted to disrupt hydrophobic interactions between Phe564 (helix H) and Ubc9 Ala131 and Tyr134 (helix C). K567A would disrupt interactions between the Lys567 Nϵ atom and the backbone carbonyl oxygen of Ubc9 Gln126 (3.4 Å), as well as VDW interactions with Pro128 and Tyr134. These mutations, combined with the structural analysis, reveal a large interface utilized in RanGAP1-Ubc9 interaction, suggesting that RanGAP1 has developed additional binding surfaces for Ubc9 that may substitute directly for an E3-like cofactor.

Functional Characterization of Ubc9

To assess Ubc9-substrate recognition, interactions observed in the Ubc9-RanGAP1 complex were used to design 19 mutations covering Ubc9 surfaces that included most of the Ubc9 catalytic and binding motifs. Mutants were expressed, purified, and assayed in SUMO conjugation assays over several time points with the C-terminal domain of RanGAP1 (Figures 2B, 6B, and 7B; see Experimental Procedures).

Mutation of the active site cysteine (C93S) diminished conjugation to an undetectable level, likely through disruption of E1-E2 SUMO transfer. Although some serine substituted E2s function in E1 modifier transfer, we have determined that C93S mutation blocks efficient SUMO transfer between E1 and Ubc9 at physiological pH (data not shown). Ubc9 mutants such as Q139A and S89AT91A exhibited nearly wild-type activity in RanGAP1 conjugation assays. Gln139 is located at the periphery of the interface (light blue in Figure 7B). The S89AT91A mutant was more active than either S89A or T91A alone, suggesting the formation of a less restrictive hydrogen-bonding network that could enable other productive binding configurations.

Several Ubc9 mutants did not exhibit wild-type rates for accumulation of sumoylated substrate but were sufficient for conjugation within the time course (blue in Figure 7B). Glu98 and Asp100 are located on the loop between strand 7 and helix B and are in a position to interact with substrates approaching the active site. Lys74, Ser89, and Thr91 interact with RanGAP1 Glu528 of the consensus motif, and Y134F, T135A, and T135L are all located between Ubc9 helix C and RanGAP1 helix H (Figure 4C).

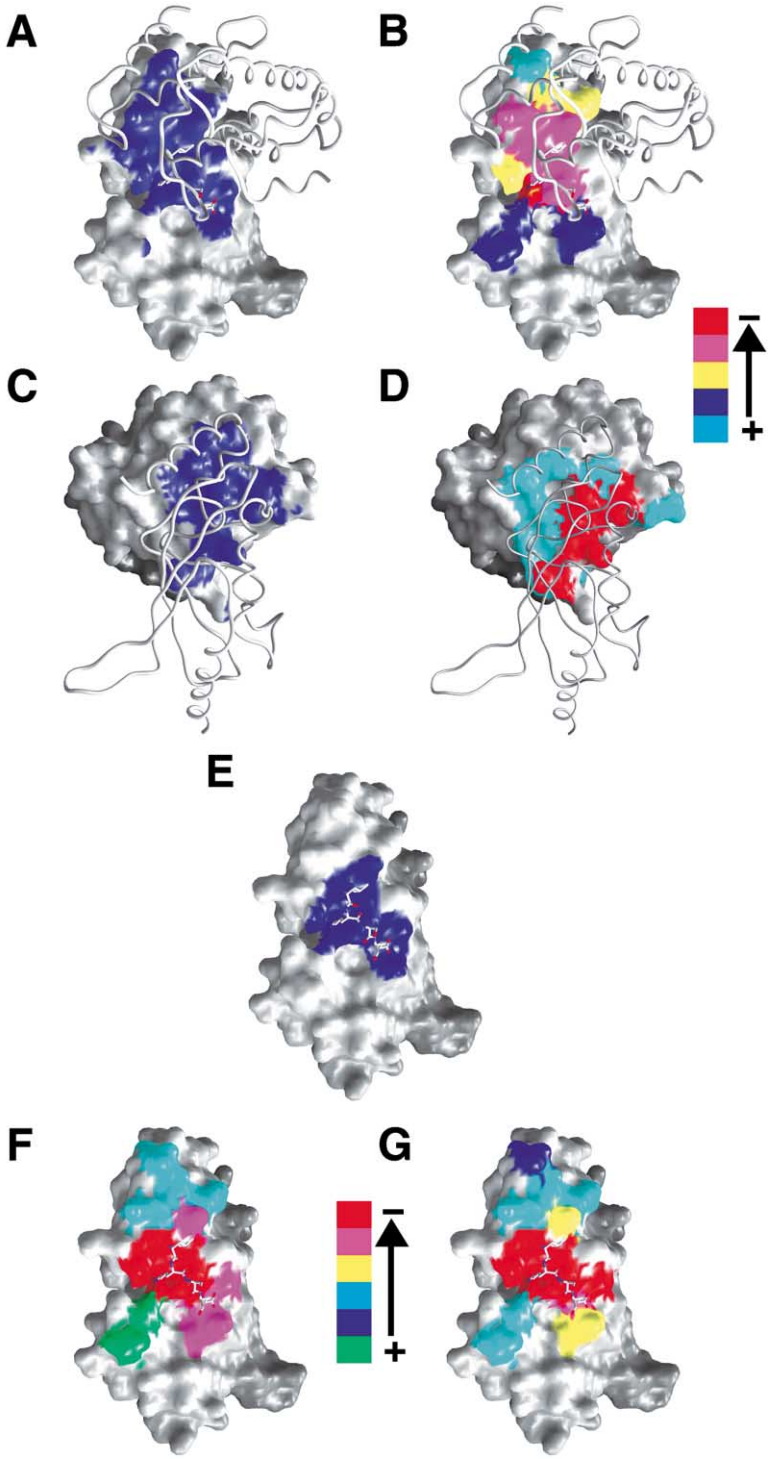

Figure 7. Surface Views of the Ubc9-RanGAP1 Interface

(A) Ubc9 surface and worm model for RanGAP1, buried Ubc9 surface area colored blue. RanGAP1 Leu525, Lys526, and Glu528 are in solid bonds.

(B) As in (A), except surface area color-coded to represent the Ubc9-RanGAP1 mutational analysis. Color-coded bar between (B) and (D) indicates activity levels from light blue (active) to red (inactive). These include Q139 (light blue); K74, S89, T91, E98, and D100 (blue); D127, E132, and T135 (yellow); Y87, P128, A129, A131, and Y134 (pink); and C93 (red).

(C) RanGAP1 surface and Ubc9 worm depicting buried RanGAP1 surface area (blue).

(D) As in (C), but with RanGAP1 mutants depicted by color. L524, L525, K526, E528, F564, and K567 (red for inactive); N512, T516, R517, I520, H521, M522, D529, I531, L537, L560, A563, and N569 (light blue for active).

(E) Ubc9 surface with RanGAP1 SUMO motif L-K-S-E in solid bonds with buried Ubc9 surface area colored blue.

(F) As in (E), but with Ubc9 mutational analysis from p53 conjugation represented as surface colors. Color-coded bar shown between (F) and (G) indicates activity levels from green (hyperactive) to red (inactive). Residues include E98 and D100 (green); E132, Y134, T135, and Q139 (light blue); K74, S89, and A131 (pink); and Y87, T91, C93, D127, P128, and A129 (red).

(G) Color-coded mutational analysis for IκBα conjugation as in (F). Residues include E98, D100, E132, Y134, and T135 (light blue); Q139 (blue); K74 and A131 (yellow); and Y87, S89, T91, C93, D127, P128, and A129 (red).

Two mutations, Y87F and D127A, were designed to assess catalytic roles for the tyrosine hydroxyl or aspartic acid carboxylate. Y87F would eliminate the tyrosine hydroxyl while preserving the hydrophobic aromatic contacts observed between Tyr87 and RanGAP1 Lys526, Ser527, and Glu528. Asp127 is in direct contact with Lys526 through a hydrogen bonding or salt-bridging interaction, potentially coordinating the lysine for attack at the thioester adduct (Figure 4). The activities observed for Y87F and D127A suggest they are not essential catalytic residues for RanGAP1 conjugation.

Several mutations exhibited detrimental effects on RanGAP1 SUMO conjugation (pink in Figure 7B). E132A and Y134A likely disrupt interactions between helix C and RanGAP1 helices H and F (Figure 4C). Mutation of Pro128, Ala129, and Ala131 also diminish SUMO conjugation of RanGAP1. These residues are all located in the loop preceding helix C that directly interacts with

RanGAP1 residues Leu525 and Lys526. Pro128 is conserved throughout the E2 family and is likely required at this position for its unique structural attributes (Figure 2B). A129C probably disrupts VDW interactions between Ubc9 and the substrate lysine by altering the backbone configuration at this position. Comparison between Y87A and Y87F reveals a significant contribution made by the aromatic ring to activity, interactions that include VDW contacts with the K-x-D/E portion of the SUMO motif. No single Ubc9 mutation other than C93S completely inhibited SUMO conjugation, suggesting that residues probed by our mutagenesis are not essential for catalytic activity. These results are consistent with the proposed model that excludes a specific E2 general base for activation of the catalytic lysine during conjugation.

Comparison between RanGAP1, IκBα, and p53

To assess general motifs utilized in Ubc9 substrate interactions and to enable a comparative analysis between respective Ubc9-substrate pairs, Ubc9 mutants were evaluated in SUMO conjugation assays with two other substrates, full-length human IκBα and the C-terminal tetramerization domain from human p53 (see Experimental Procedures). The RanGAP1 sumoylation motif occurs between secondary structural elements (Figures 2 and 3). In contrast, sumoylation motifs within IκBα (DGLKKERL) and p53 (LMFKTEGP) occur at N- and C-terminal ends of the proteins, respectively. p53 Lys386 is targeted for sumoylation and is located within a C-terminal peptide outside the structured tetramerization domain (residues 325–356) (Jeffrey et al., 1995). IκBα Lys21 is targeted for both sumoylation by Ubc9 and for ubiquitination by UbcH5b, UbcH5c, and Ubc3 (Gonen et al., 1999), and it occurs N-terminal to the structured ankyrin repeats found in this protein (Huxford et al., 1998; Jacobs and Harrison, 1998).

Analysis of SUMO conjugation reactions for p53, RanGAP1, and IκBα reveals more similarities than differences among these substrates with respect to individual Ubc9 mutations, although conjugation reactions containing IκBα and p53 more closely resemble each other when compared to RanGAP1. Taken together, these results indicate a central role for Ubc9 recognition of the SUMO Ψ-K-x-D/E motif in Ubc9-substrate interactions. They also suggest that Ubc9 does not discriminate significantly among internal, N-terminal, or C-terminal consensus sites within respective targets. Interestingly, some Ubc9 mutants that exhibited activity in RanGAP1 assays were almost completely defective in p53 and IκBα conjugation, and others that reduced catalytic activity in RanGAP1 conjugation did not affect conjugation to p53 or IκBα (Figures 6B–6D).

Several Ubc9 mutations elicit wild-type activity in assays with p53 or IκBα (blue in Figures 7F and 7G), and some mutations apparently enhance the process (E98A and D100A, green in Figure 7F for p53). Although untested, E98A and D100A could make the surface of Ubc9 more hydrophobic in character, thus increasing binding interactions for this enzyme-substrate pair. Mutations in Ubc9 helix C, such as Y134A and E132A, interfere with RanGAP1 SUMO transfer by disrupting a binding interface between these molecules. Ubc9 mutations in this region have little to no effect on SUMO conjugation of IκBα and p53, suggesting that IκBα and p53 do not interact with Ubc9 through the same interface utilized by RanGAP1.

Ubc9 mutations that dramatically decrease IκBα and p53 SUMO conjugation include residues predicted to make direct contact with the consensus Ψ-K-x-D/E motif, as observed in the Ubc9-RanGAP1 structure (Figures 4 and 7E–7G). Though not critical for RanGAP1 sumoylation, Asp127 is required for effective IκBα and p53 sumoylation, probably due to its direct contact with the acceptor lysine, one that likely positions the lysine for attack at the thioester adduct. Tyr87 contacts the K-x-D/E portion of the motif through VDW interactions with each of these residues, and substitution of the side chain to alanine effectively blocks conjugation. Ala129 contacts the acceptor lysine through VDW contacts, and both Pro128 and Ala131 provide VDW surfaces for interaction with the Ψ residue of the motif. Lys74, Ser89, and Thr91 all interact with the acidic residue of the Ψ-K-x-D/E motif, and each is required for full activity.

Ubc9 residues observed in direct contact with the RanGAP1 SUMO motif are apparently more critical for Ubc9 interaction with p53 and IκBα, as the Ubc9 surface area buried by this motif is almost perfectly covered by the detrimental mutations that affect p53 and IκBα SUMO conjugation (Figures 7E–7G). E2 enzymes known to conjugate ubiquitin to IκBα Lys21 share some sequence similarity to Ubc9 within the motif recognition interface. These include Ubc9 residues Tyr87, Thr89, and Ala129 for Ubc3 and Ubc9 residues Lys74, Ser91, and Asp127 for UbcH5b (Figure 2B), indicating that Ubc3 and UbcH5b may recognize the peptide containing IκBα Lys21 in a similar manner. While speculative and untested, these observations can be extended to suggest that other E2-mediated conjugation reactions coordinate their lysine-containing substrates in a manner similar to that observed in the Ubc9-RanGAP1 complex.

Conclusions

We have presented the crystal structure and biochemical analysis of a complex between Ubc9 and the C-terminal domain of RanGAP1, the first E2-substrate complex observed at atomic resolution. Analysis of the RanGAP1 C-terminal domain reveals structural similarity to proteins with helical repeat motifs, although the functional significance of these relationships with respect to SUMO conjugation is limited since none contain a consensus SUMO motif. Analysis of the complex revealed extensive RanGAP1 interactions with Ubc9 surfaces outside the consensus motif, an adaptation that likely results in increased binding and more effective SUMO transfer as compared to other known substrates. The structure revealed key determinants for Ubc9 recognition of the Ψ-K-x-D/E consensus sumoylation motif that is observed within all known SUMO-modified proteins. Shallow grooves, complementary electrostatic, and hydrogen bonding interactions created by conserved residues on the surface of Ubc9 provide a platform onto which the Ψ-K-x-D/E motif is saddled and specifically recognized, enabling proper orientation and coordination of the acceptor lysine.

The structure and corresponding mutagenesis sug-

gests that residues surrounding the active site cysteine are not capable of specifically removing a proton from the acceptor lysine during nucleophilic attack at the thioester adduct. Although the acceptor lysine is often thought of as a substrate, lysine serves as the nucleophile within a three-part enzyme complex that includes the "substrate" and the Ubc9-SUMO thioester, an intermediate analogous to the acyl-enzyme complex thought to occur during protease reactions. Since the thioester is relatively unstable, the lysine may merely need to approach the thioester in the correct orientation for attack, thus eliminating the need for specific removal of a lysine proton by E2. Although a lowered pK_a for the nucleophilic lysine cannot be excluded, we do not believe that the lysine is activated by a general base, but rather that it is facilitated for attack through proper orientation with respect to the thioester.

Structure-based mutagenesis and SUMO conjugation assays with Ubc9, IκBα, p53, and RanGAP1 have revealed a similar mode of interaction between Ubc9 and respective Ψ-K-x-D/E motifs, suggesting that substrates containing this motif will interact with Ubc9 in a similar manner. While we are not able to exclude additional Ubc9 surfaces utilized for p53 and IκBα binding, mutations that fully disrupt p53 and IκBα sumoylation exhibit activity against RanGAP1, suggesting that RanGAP1 encodes an additional E3-like binding activity capable of recruiting Ubc9 to its Ψ-K-x-D/E motif for SUMO conjugation. These results are consistent with mechanisms for E2- and E3-mediated conjugation that utilize SP-ring E3-like proteins to increase activity by enhancing Ubc9-substrate affinities. The structural and biochemical results presented here should provide further groundwork for studies focused on Ubc9 E2-mediated SUMO conjugation and, more generally, for studies related to substrate recognition by cognate E2 conjugation enzymes.

Experimental Procedures

Cloning, Expression, and Protein Purification

Human *UBC9* was amplified from cDNA by PCR, cloned into pET-28b to encode an N-terminal thrombin cleavable hexahistidine tagged fusion protein (phUbc9), transformed into *E. coli* BL21(DE3)-pLysS (Novagen), and induced with IPTG. Protein was purified by Ni-NTA-agarose resin (Qiagen), dialyzed against 50 mM Tris-HCl (pH 8.0), 200 mM NaCl, 2 mM β-mercaptoethanol (BME), and bovine thrombin (Sigma), and purified by cation exchange (MonoS, Pharmacia). Mouse RanGAP1(420–589)p was amplified by PCR and cloned into a modified pET28b vector containing N-terminal hexahistidine-tagged *S. cerevisiae* Smt3 (pSUMO) (Mossessova and Lima, 2000). Smt3-RanGAP(420–589)p was purified by metal-affinity, cleaved by Ulp(403–621)p, and purified by gel filtration (Superdex 75).

Selenomethionyl (SeMet) protein was produced in *E. coli* DL41 (Hendrickson et al., 1990). Purified RanGAP1 and Ubc9 were mixed 1:1, purified by gel filtration (Superdex75), and concentrated to 10 mg/ml in 50 mM NaCl, 10 mM Tris-HCl (pH 8.0), 1 mM BME. Coding regions for full-length human IκBα and p53(320–393)p were amplified by PCR from cDNA, cloned into pSUMO, expressed and purified as for RanGAP1, further purified by ion-exchange (MonoS-p53, MonoQ-IκBα), and concentrated (10 mg/ml) in 100 mM NaCl, 50 mM Tris-HCl (pH 8.0), 1 mM BME. Proteins were aliquoted, frozen in liquid nitrogen, and stored at −80°C.

Crystallographic Analysis

Ubc9-RanGAP1 crystals were obtained by hanging drop vapor diffusion against 1.0 M lithium sulfate, 0.5 M ammonium sulfate, 50 mM sodium citrate (pH 5.5) and 5% glycerol, cryoprotected by addition of 25% glycerol, and cryopreserved in liquid nitrogen. SeMet crystals diffracted X-rays weakly to 2.6 Å along the *c* axis and to 3.0 Å along *a* and *b* axes ($P3_221$, a = b = 128.9 Å, c = 130.3 Å, α = β = 90°, γ = 120°). A second crystal form was obtained from 2.0 M ammonium phosphate, 0.1 M HEPES (pH 7.0), 10 mM $CuCl_2$, 5% glycerol ($P2_12_12$, a = 86.5 Å, b = 126.5 Å, c = 72.6 Å, α = β = γ = 90°) that diffracted anisotropic X-rays to 2.3 Å.

Diffraction screening utilized a Cu-Kα source (Rigaku RU200) equipped with Osmic multilayer optics and a Raxis-IV imaging plate detector. Native and MAD data sets were collected at National Synchrotron Light Source (Brookhaven, NY) beamline X4A using an ADSC Quantum-4 detector. Data was reduced with DENZO, SCALEPACK (Otwinowski and Minor, 1997) and CCP4 (Collaborative Computational Project, 1994) (Table 1).

MAD data analysis revealed seven selenium sites used to generate 2.8 Å phases (SOLVE and RESOLVE [Terwilliger and Berendzen, 1999]). The model was traced using O (Jones et al., 1991) and refined with CNS (Brunger et al., 1998). Structures for two complexes using the $P2_12_12$ data set were solved by molecular replacement to 2.5 Å, refined without noncrystallographic symmetry, and manually rebuilt into $2F_o-F_c$, F_o-F_c, and simulated annealing OMIT maps. The model, having excellent geometry with no Ramachandran outliers, contained residues 3–158 for Ubc9 and 434–589 for RanGAP1. Electron density for Ubc9 residues 1 and 2 and RanGAP1 residues 420–433 were not observed. These regions represent ~5% of the structure, possibly contributing to the relative high R_{free} value obtained in refinement. Coordinates and structure factors are deposited in the Protein Data Bank with accession code 1KPS.

Mutagenesis and Biochemical Assays

Point mutations in the C-terminal domain of RanGAP1 were engineered into NΔ419/PK (Sampson et al., 2001) using PCR-based mutagenesis. Proteins were translated in rabbit reticulocyte lysate in the presence of [^{35}S]methionine. SUMO-1 modification by endogenous reticulocyte lysate-conjugating enzymes was determined by SDS-PAGE and autoradiography. Point mutations in phUbc9 were obtained using PCR-based mutagenesis (QuikChange, Stratagene). Mutants were expressed and purified as for wild-type Ubc9 and concentrated to ~1 mg/ml in 350 mM NaCl, 20 mM Tris-HCl (pH 8.0), 1 mM DTT. SUMO conjugation was assayed at 37°C with RanGAP1(420–589)p using 0.3 μM E1, 2 mM ATP, 5 mM $MgCl_2$, 10% glycerol, 50 mM Tris (pH 7.5), 2 μM RanGAP1, and 2 μM mature SUMO and initiated by adding 0.3 μM Ubc9. Samples were removed at specified times, denatured in SDS-PAGE buffer, and stored at 4°C or −20°C until SDS-PAGE analysis and Coomassie blue staining. p53 and IκBα SUMO conjugation were assayed identically except that substrate and SUMO concentrations were increased to 50 μM and Ubc9 to 3 μM. *UBC9* mutations were confirmed by DNA sequencing.

Acknowledgments

We thank John Buglino, Vincent Shen, and David R. Lima for technical assistance and the staff of beamline X4A at the National Synchrotron Light Source, a DOE facility. Beamline X4A is supported by the Howard Hughes Medical Institute. M.J.M. and D.A.S. are supported by a grant from the National Institutes of Health (GM60980). V.B.V. acknowledges support from the Secretaría de Estado de Educación y Universidades de Spain. C.D.L. acknowledges support from the Arnold and Mabel Beckman Foundation.

Received November 19, 2001; revised January 4, 2002.

References

Brunger, A.T., Adams, P.D., Clore, G.M., DeLano, W.L., Gros, P., Grosse-Kunstleve, R.W., Jiang, J.S., Kuszewski, J., Nilges, M., Pannu, N.S., et al. (1998). Crystallography & NMR system: a new software suite for macromolecular structure determination. Acta Crystallogr. D *54*, 905–921.

CCP4 (Collaborative Computational Project) (1994). The CCP4 suite:

programs for protein crystallography. Acta Crystallogr. D *50*, 760–763.

Desterro, J.M., Rodriguez, M.S., and Hay, R.T. (1998). SUMO-1 modification of IκBα inhibits NF-κB activation. Mol. Cell *2*, 233–239.

Evans, S.V. (1993). SETOR: hardware-lighted three-dimensional solid model representations of macromolecules. J. Mol. Graph. *11*, 134–138.

Gonen, H., Bercovich, B., Orian, A., Carrano, A., Takizawa, C., Yamanaka, K., Pagano, M., Iwai, K., and Ciechanover, A. (1999). Identification of the ubiquitin carrier proteins, E2s, involved in signal-induced conjugation and subsequent degradation of IκBα. J. Biol. Chem. *274*, 14823–14830.

Gostissa, M., Hengstermann, V.F., Sandy, P., Schwarz, S.E., Scheffner, M., and Sal, G.D. (1999). Activation of p53 by conjugation to the ubiquitin-like protein SUMO-1. EMBO J. *18*, 6462–6471.

Hamilton, K.S., Ellison, M.J., Barber, K.R., Williams, R.S., Huzil, J.T., McKenna, S., Ptak, C., Glover, M., and Shaw, G.S. (2001). Structure of a conjugating enzyme-ubiquitin thiolester intermediate reveals a novel role for the ubiquitin tail. Structure *9*, 897–904.

Hendrickson, W.A. (1991). Determination of macromolecular structures from anomalous diffraction of synchrotron radiation. Science *254*, 51–58.

Hendrickson, W.A., Horton, J.R., and LeMaster, D.M. (1990). Selenomethionyl proteins produced for analysis by multiwavelength anomalous diffraction (MAD): a vehicle for direct determination of three-dimensional structure. EMBO J. *9*, 1665–1672.

Hershko, A., and Ciechanover, A. (1998). The ubiquitin system. Annu. Rev. Biochem. *67*, 425–479.

Hillig, R.C., Renault, L., Vetter, I.R., Drell, T., 4th, Wittinghofer, A., and Becker, J. (1999). The crystal structure of rna1p: a new fold for a GTPase-activating protein. Mol. Cell *3*, 781–791.

Hochstrasser, M. (1996). Ubiquitin-dependent protein degradation. Annu. Rev. Genet. *30*, 405–439.

Hochstrasser, M. (2001). SP-RING for SUMO. New functions bloom for a ubiquitin-like protein. Cell *5*, 5–8.

Holm, L., and Sander, C. (1993). Protein structure comparison by alignment of distant matrices. J. Mol. Biol. *233*, 123–138.

Huang, L., Kinnucan, E., Wang, G., Beaudenon, S., Howley, P.M., Huibregtse, J.M., and Pavletich, N.P. (1999). Structure of an E6AP-UbcH7 complex: insights into ubiquitination by the E2–E3 enzyme cascade. Science *286*, 1321–1326.

Huxford, T., Huang, D.B., Malek, S., and Ghosh, G. (1998). The crystal structure of the IκBα/NF-κB complex reveals mechanisms of NF-kappaB inactivation. Cell *95*, 759–770.

Jacobs, M.D., and Harrison, S.C. (1998). Structure of an IκBα/NF-κB complex. Cell *95*, 749–758.

Jeffrey, P.D., Gorina, S., and Pavletich, N.P. (1995). Crystal structure of the tetramerization domain of the p53 tumor suppressor at 1.7 Å. Science *267*, 1498–1502.

Johnson, E.S., and Blobel, G. (1997). Ubc9p is the conjugating enzyme for the ubiquitin-like protein Smt3p. J. Biol. Chem. *272*, 26799–26802.

Johnson, E.S., and Blobel, G. (1999). Cell cycle-regulated attachment of the ubiquitin-related protein SUMO to the yeast septin. J. Cell Biol. *147*, 981–993.

Johnson, E.S., and Gupta, A.A. (2001). An E3-like factor that promotes SUMO conjugation to the yeast septins. Cell *106*, 735–744.

Jones, T.A., Zou, J.Y., Cowan, S.W., and Kjeldgaard, M. (1991). Improved methods for building protein models in electron density maps and the location of errors in these models. Acta Crystallogr. A *47*, 110–118.

Kahyo, T., Nishida, T., and Yasuda, H. (2001). Involvement of PIAS1 in the sumoylation of tumor suppressor p53. Mol. Cell *8*, 713–718.

Kamitani, T., Kito, K., Nguyen, H.P., Wada, H., Fukuda-Kamitani, T., and Yeh, E.T. (1998). Identification of three major sentrinization sites in PML. J. Biol. Chem. *273*, 26675–26682.

Laney, J.D., and Hochstrasser, M. (1999). Substrate targeting in the ubiquitin system. Cell *97*, 427–430.

Li, S.-J., and Hochstrasser, M. (1999). A new protease required for cell cycle progression in yeast. Nature *398*, 246–251.

Mahajan, R., Delphin, C., Guan, T., Gerace, L., and Melchior, F. (1997). A small ubiquitin-related polypeptide involved in targeting RanGAP1 to nuclear pore complex protein RanBP2. Cell *88*, 97–107.

Matunis, M.J., Coutavas, E., and Blobel, G. (1996). A novel ubiquitin-like modification modulates the partitioning of the Ran-GTPase-activating protein RanGAP1 between the cytosol and the nuclear pore complex. J. Cell Biol. *135*, 1457–1470.

Melchior, F. (2000). SUMO-nonclassical ubiquitin. Annu. Rev. Cell Dev. Biol. *16*, 591–626.

Meluh, P.B., and Koshland, D. (1995). Evidence that the MIF2 gene of *Saccharomyces cerevisiae* encodes a centromere protein with homology to the mammalian centromere protein CENP-C. Mol. Biol. Cell *6*, 793–807.

Mossessova, E., and Lima, C.D. (2000). Ulp1-SUMO crystal structure and genetic analysis reveal conserved interactions and a regulatory element essential for cell growth in yeast. Mol. Cell *5*, 865–876.

Muller, S., Hoege, C., Pyrowolakis, G., and Jentsch, S. (2001). SUMO, ubiquitin's mysterious cousin. Nat. Rev. Mol. Cell Biol. *2*, 202–210.

Nicholls, A., Sharp, K.A., and Honig, B. (1991). Protein folding and association: insights from the interfacial and thermodynamic properties of hydrocarbons. Proteins *11*, 281–296.

Otwinowski, Z., and Minor, W. (1997). Processing of X-ray diffraction data collected in oscillation mode. In Methods in Enzymology, Volume 276, C.W. Carter, Jr. and R.M. Sweet, eds. (New York: Academic Press), pp. 307–326.

Rodriguez, M.S., Desterro, J.M.P., Lain, S., Midgley, C.A., Lane, D.L., and Hay, R.T. (1999). SUMO-1 modification activates the transcriptional response of p53. EMBO J. *18*, 6455–6461.

Saitoh, H., Pu, R.T., and Dasso, M. (1997). SUMO-1: wrestling with a new ubiquitin-related modifier. Trends Biochem. Sci. *22*, 374–376.

Sampson, D.A., Wang, M., and Matunis, M.J. (2001). The small ubiquitin-like modifier-1 (SUMO-1) consensus sequence mediates Ubc9 binding and is essential for SUMO-1 modification. J. Biol. Chem. *276*, 21664–21669.

Seufert, W., Futcher, B., and Jentsch, S. (1995). Role of a ubiquitin-conjugating enzyme in degradation of S- and M-phase cyclins. Nature *373*, 78–81.

Sternsdorf, T., Jensen, K., and Will, H. (1997). Evidence for covalent modification of the nuclear dot-associated proteins PML and Sp100 by PIC1/SUMO-1. J. Cell Biol. *139*, 1621–1634.

Takahashi, Y., Iwase, M., Konishi, M., Tanaka, M., Toh-e, A., and Kikuchi, Y. (1999). Smt3, a SUMO-1 homolog, is conjugated to cdc3, a component of septin rings at the mother-bud neck in budding yeast. Biochem. Biophys. Res. *259*, 582–587.

Takahashi, Y., Toh-e, A., and Kikuchi, Y. (2001). A novel factor required for the SUMO1/Smt3 conjugation of yeast septins. Gene *275*, 223–231.

Tanaka, K., Nishide, J., Okazaki, K., Kato, H., Niwa, O., Nakagawa, T., Matsuda, H., Kawamukai, M., and Murakami, Y. (1999). Characterization of a fission yeast SUMO-1 homologue, Pmt3p, required for multiple nuclear events, including the control of telomere length and chromosome segregation. Mol. Cell. Biol. *19*, 8660–8672.

Terwilliger, T.C., and Berendzen, J. (1999). Automated MAD and MIR structure solution. Acta Crystallogr. D *55*, 849–861.

Tong, H., Hateboer, G., Perrakis, A., Bernards, R., and Sixma, T.K. (1997). Crystal structure of murine/human Ubc9 provides insight into the variability of the ubiquitin-conjugating system. J. Biol. Chem. *272*, 21381–21387.

VanDemark, A.P., Hofmann, R.M., Tsui, C., Pickart, C.M., and Wolberger, C. (2001). Molecular insights into polyubiquitin chain assembly: crystal structure of the Mms2/Ubc13 heterodimer. Cell *105*, 711–720.

Zheng, N., Wang, P., Jeffrey, P.D., and Pavletich, N.P. (2000). Structure of a c-Cbl-UbcH7 complex: RING domain function in ubiquitin-protein ligases. Cell *102*, 533–539.